The Origin of Infrared Marker Bands of Porphyrin π-Cation Radicals: Infrared Assignments for Cations of Copper(II) Complexes of Octaethylporphine and Tetraphenylporphine

Songzhou Hu and Thomas G. Spiro*

Contribution from the Department of Chemistry, Princeton University, Princeton, New Jersey 08544

*Received July 12, 1993**

Abstract: Oxidation of metalloporphyrins to π-cation radicals is well known to be marked by the development of strong infrared bands at ~1280 cm^{-1} for tetraphenylporphines (TPPs) and at ~1550 cm^{-1} for octaethylporphines (OEPs). The molecular basis of these marker bands is investigated by assigning the IR spectra of CuOEP and CuTPP π-cation radicals, via selective deuteration. The IR spectrum of CuTPP is also assigned for the first time. The ~1280-cm^{-1} $TPP^{\bullet+}$ marker band is assigned to ν_{41}, the pyrrole half-ring stretch, which involves out-of-phase stretching of the C_α–C_β and C_α–N bonds. The ~1550-cm $OEP^{\bullet+}$ marker band is assigned to ν_{37}, the asymmetric C_α–C_m stretching mode. In addition, a $CuOEP^{\bullet+}$ band at 1600 cm^{-1} assigned to ν_{38}, the C_β–C_β stretch, gains intensity in the $CuOEP^{\bullet+}$ spectrum and indeed becomes the strongest band when the spectrum is taken in $CDCl_3$ solution, instead of in a KBr pellet. The intensification of the cation radical marker bands is proposed to result from the matching of the normal mode eigenvectors to the antibonding pattern of the half-filled HOMOs: a_{2u} for $TPP^{\bullet+}$ and a_{1u} for $OEP^{\bullet+}$. A large dipole moment is generated across the porphyrin ring by the compression and expansion of bonds for which the HOMO contains nodes. The extra intensification of ν_{37} in solid samples of $OEP^{\bullet+}$ radicals is connected with a bond-alternate distortion that mixes a_{2u} character into the a_{1u} HOMO. In addition, skeletal mode splittings are seen for $CuOEP^{\bullet+}$ in the solid state and are attributed to dimerization; these splittings are absent for $CuTPP^{\bullet+}$, for which dimer contacts are attenuated by the bulky phenyl substituents.

Introduction

Metalloporphyrin π-cation radicals play a central role in the redox chemistry of many heme-containing enzymes and photo-induced electron-transfer processes. The best characterized examples of biological porphyrin cation radicals are those occurring in the catalytic cycles of peroxidases,[1] catalases,[2] and possibly cytochromes P450.[3] The "compound I" intermediate of these heme enzymes is a doubly oxidized product of the ferric heme produced by their reaction with hydroperoxides. It has now been firmly established that one of the two electron oxidations is centered on the heme iron, generating an oxoferryl species, while the second electron is removed from the porphyrin ring to form the green π-cation radical. Another celebrated biological cation radical is transiently created in the bacteriochlorophyll "special pair" dimer of photosynthetic bacterial reaction centers through light-induced charge separation and transfer of an electron to the neighboring bacteriopheophytin.[4]

Synthetic metalloporphyrins have been used to gain a detailed understanding of the structure and dynamics of the π-cation radicals. These oxidized species have been characterized by a number of spectroscopic techniques[5–9] and X-ray crystallography.[10] Infrared spectroscopy[11] has been frequently used to identify the porphyrin ring-oxidized π-cation radicals since the initial work by Goff, Reed, and co-workers[11a] who surveyed the IR spectra for the π-cation radicals of metalloporphyrins, including several metal complexes of tetraphenylporphine (TPP) and of octaethylporphine (OEP). They found that π-cation radical formation produced characteristic IR bands at about 1280 cm^{-1} for M(TPP)s and at about 1550 cm^{-1} for M(OEP)s. The appearance of these two modes is related to the oxidation of the porphyrin ring rather than to the oxidation of the central metal. Itoh and co-workers[11b] studied the IR spectra of the π-cation radicals of magnesium, zinc, and cobalt complexes of OEP and noted frequency changes of several other skeletal modes. However, two important questions remain to be answered. (1) What

* Abstract published in *Advance ACS Abstracts,* November 1, 1993.

(1) (a) Dunford, H. B.; Stillman, J. S. *Coord. Chem. Rev.* **1976**, *19*, 187–251. (b) Hewson, W. D.; Hager, L. P. In *The Porphyrins*; Dolphin, D., Ed.; Academic Press: New York, 1979; Vol. 7, pp 295–332.

(2) (a) Schonbaum, G. R.; Chance, B. In *Enzymes*, 3rd ed.; Academic Press: New York, 1976; Vol. 13, Chapter 7. (b) Frew, J. E.; Jones, P. *Advances in Inorganic and Bioinorganic Mechanisms*; Academic Press: Orlando, FL, 1984; Vol. 3, pp 175–212.

(3) (a) White, R. E.; Coon, M. J. *Annu. Rev. Biochem.* **1980**, *49*, 315. (b) Guengerich, F. P.; McDonald, T. L. *Acc. Chem. Res.* **1984**, *17*, 9–16. (c) Murray, R. I.; Fisher, M. T.; Debrunner, G.; Sligar, S. G. In *Metalloproteins Part I: Metal Proteins with Redox Roles*; Harrison, P. M., Ed.; Verlag Chemie: Weinheim, 1985; p 157. (d) Ortiz de Montellano, P. R., Ed. *Cytochrome P450 Structure, Mechanism, and Biochemistry*; Plenum Press: New York, 1986. (e) Dawson, J. H.; Eble, K. S. *Adv. Inorg. Bioinorg. Mech.* **1986**, *4*, 1–64. (f) Black, S. D.; Coon, M. J. *Adv. Enzymol. Relat. Areas Mol. Biol.* **1987**, *60*, 35–87. (g) Dawson, J. H. *Science* **1988**, *240*, 433–439. (h) Dawson, J. H.; Sono, M. *Chem. Rev.* **1987**, *87*, 1255–1276. (i) Schuster, I., Ed. *Cytochrome P450: Biochemistry and Biophysics*; Taylor & Francis: Bristol, PA, 1989.

(4) Scheer, H. Ed. *Chlorophylls*; CRC: Boca Raton, FL, 1991.

(5) (a) Fuhrhop, J.-H.; Mauzerall, D. *J. Am. Chem. Soc.* **1969**, *91*, 4174–4181. (b) Fuhrhop, J.-H.; Wasser, P.; Riesner, D. Mauzerall, D. *J. Am. Chem. Soc.* **1972**, *94*, 7996–8001.

(6) (a) Goff, H. M.; Phillippi, M. A. *J. Am. Chem. Soc.* **1983**, *105*, 7567–7571. (b) Godziela, G. M.; Goff, H. M. *J. Am. Chem. Soc.* **1986**, *108*, 2237–2243. (c) Morishima, I.; Takamuki, Y.; Shiro, Y. *J. Am. Chem. Soc.* **1984**, *106*, 7666–7672.

(7) (a) Browett, W. R.; Stillman, M. J. *Inorg. Chim. Acta* **1981**, *49*, 69–77. (b) Browett, W. F.; Stillman, M. J. *Biochim. Biophys. Acta* **1981**, *660*, 1–7. (c) Gasyna, Z.; Browett; W. R.; Stillman, M. J. *Inorg. Chem.* **1988**, *27*, 4619–4622.

(8) Fajer, J.; Davis, M. S. *In The Porphyrins*; Dolphin, D., Ed.; Academic Press: New York, 1978; Vol. 4, pp 197–256.

(9) (a) Yamaguchi, H.; Nakano, M.; Itoh, K. *Chem. Lett.* **1982**, 1397–1400. (b) Kim, D.; Miller, L. A.; Rakhit, G.; Spiro, T. G. *J. Phys. Chem.* **1986**, *90*, 3320–3325. (c) Czernuszewicz, R. S.; Macor, K. A.; Li, X.-Y.; Kincaid, J. R.; Spiro, T. G. *J. Am. Chem. Soc.* **1989**, *111*, 3860–3869. (d) Macor, K. A.; Czernuszewicz, R. S.; Spiro, T. G. *Inorg. Chem.* **1990**, *29*, 1996–2000. (e) Salehi, A.; Oertling, W. A.; Babcock, G. T.; Chang, C. K. *J. Am. Chem. Soc.* **1986**, *108*, 5630–5631. (f) Oertling, W. A.; Salehi, A.; Chang, C. K.; Babcock, G. T. *J. Phys. Chem.* **1987**, *91*, 3114–3116. (g) Oertling, W. A.; Salehi, A.; Chung, Y. C.; Leroi, G. E.; Chang, C. K.; Babcock, G. T. *J. Phys. Chem.* **1987**, *91*, 5887–5898. (h) Oertling, W. A.; Salehi, A.; Chang, C. K.; Babcock, G. T. *J. Phys. Chem.* **1989**, *93*, 1311–1319. Hashimoto, S.; Mizutani, Y.; Tatsuno, Y.; Kitagawa, T. *J. Am. Chem. Soc.* **1991**, *113*, 6542–6549.

0002-7863/93/1515-12029$04.00/0

is the nature of the normal modes giving rise to the signature bands, and (2) why do certain bands undergo strong intensification upon π-cation radical formation?

In this work, we analyze the FT-IR spectra of the π-cation radicals of CuTPP and CuOEP using their pyrrole-d_8, phenyl-d_{20}, and *meso*-d_4 isotopomers. The infrared spectrum of neutral CuTPP is also assigned for the first time. On the basis of this analysis, π-cation radical marker bands are assigned to the porphyrin skeletal modes ν_{41} for CuTPP and ν_{37} and ν_{38} for CuOEP. The increased intensities of these marker bands are explained by the a_{1u} and a_{2u} radical character because the antibonding nodal patterns are found to match the vibrational eigenvectors of the asymmetric C_α–C_m (ν_{37}), the C_β–C_β (ν_{38}), and the symmetrical pyrrole half-ring (ν_{41}) stretches.

Experimental Section

Octaethylporphine (OEP), CuOEP, and CuTPP were obtained from Midcentury (Posen, IL). *meso*-d_4 OEP was obtained by exchange of the methine hydrogens in 9:1 D_2SO_4/D_2O for 20 h at room temperature. The deuterated product was isolated by extracting the neutralized porphyrin with methylene chloride. Greater than 95% deuteration was accomplished, as evidenced from the NMR spectrum. The pyrrole-d_8 TPP and phenyl-d_{20} TPP isotopomers were synthesized according to the method of Lindsey et al.,[12] commencing with pyrrole-d_8 or benzaldehyde-d_5 (both from Carbridge Isotope Laboratories, Woburn, MA), respectively. Tetraphenylchlorin, present in traces, was dehydrogenated by treatment with 2,3-dichloro-5,6-dicyanobenzoquinone as described.[12] Copper was inserted into each free base in boiling DMF and purified by passing through an alumina column.

The π-cation radicals were prepared by treating 5 mg of CuTPP or CuOEP in 3 mL of dried methylene chloride with 1.2-fold tris(4-bromophenyl)aminium hexachloroantimonate (Aldrich, Milwaukee, WI) under nitrogen. After the solution has been stirred for about 10 min for CuOEP and 1 h for CuTPP, the volume of the solution was reduced to about 0.5 mL, to which was then added 10 mL of chilled pentane. The precipitated π-cation radicals were then collected by centrifugation, washed three times with chilled pentane, and dried in a desiccator overnight. The electronic absorption spectra of the cation radicals of CuOEP and CuTPP agree with those reported.[10c]

FT-IR spectra were obtained with a Nicolet FT 730 fourier transform infrared spectrometer. The spectral resolution was set at 2 cm^{-1}. Samples were either prepared as KBr pellets or dissolved in chloroform-*d*. For solution samples, calcium fluoride windows (Spectra-Tech, Stamford, CT) were used.

Results

A. CuOEP. Figure 1 shows the FT-IR spectra (900–1700 cm^{-1}) of the π-cation radicals of natural abundance CuOEP and its *meso*-d_4 isotopomer, along with the spectrum of neutral CuOEP for comparison. The dotted lines correlate corresponding modes, as judged from their intensity pattern and isotope shifts. Mode assignments are indicated in the figure and are listed in Table I, along with the isotope shifts. The assignments were made by analogy to those of NiOEP, for which a complete normal mode analysis has been performed.[13] Substitution of nickel with copper is expected to shift some of the skeletal mode frequencies but not to substantially modify the form of the normal modes.

Assignment of the two highest frequency E_u modes deserves special comment. They are ν_{37} and ν_{38}, which arise from the

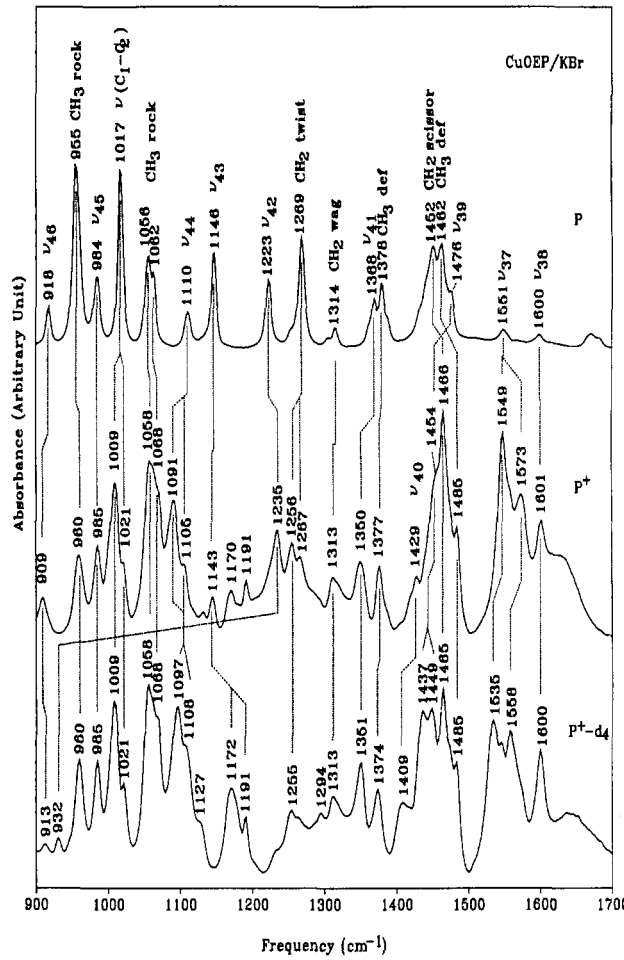

Figure 1. FT-IR spectra of the π-cation radicals for natural abundance (P^+), *meso*-d_4 (P^+-d_4), and neutral (P) CuOEP in KBr pellets.

Table I. Infrared Frequencies and Their Normal Mode Assignments of CuOEP and Its Cation Radicals

CuOEP		CuOEP cation radical		
na[a]	*meso*-d_4	na	*meso*-d_4	assignment
1600	1599	1601	1600	ν_{38} $\nu(C_\beta$–$C_\beta)$
1551	1538	1573/1549	1558/1535	ν_{37} $\nu(C_\alpha$–$C_m)_{asym}$
1476	1471	1454	1449/1436	ν_{39} $\nu(C_\alpha$–$C_m)_{sym}$
1462	1460	1485	1485	CH_3 def (out-of-phase)
1452	1450	1466	1466	CH_2 scissor
		1429	1409	ν_{40} ν(pyr quarter ring)
1378	1379	1377	1374	CH_3 def (in-phase)
1368	1368	1350	1351	ν_{41} ν(pyr half ring)$_{sym}$
1314	1314	1313	1313/1294	CH_2 wag
1269	1262	1256/1267	1255/1265	CH_2 twist
1223	945	1235	932	ν_{42} $\delta(C_mH)$
1146	1181	1143	1172/1191	ν_{43} $\nu(C_\beta$–$C_1)_{sym}$
1110	1145	1091/1105	1097/1108	ν_{44} ν(pyr half ring)$_{asym}$
1056/1062	1056/1062	1058/1068	1058/1068	CH_3 rock
1017	1019	1009/1021	1009/1021	$\nu(C_1$–$C_2)$
984	984	985	985	ν_{45} $\nu(C_\beta$–$C_1)_{asym}$
955	958	960	960	CH_3 rock
918	908	909	913	ν_{46} δ(pyr)$_{sym}$

[a] na = natural abundance.

(10) (a) Spaulding, L. D.; Eller, P. G.; Bertrand, J. A.; Felton, R. H. *J. Am. Chem. Soc.* **1974**, *96*, 982–987. (b) Buisson, G.; Deronzier, A.; Duee, E.; Gans, P.; Marchon, J.-C.; Regnard, J.-R. *J. Am. Chem. Soc.* **1982**, *104*, 6793–6796. (c) Scholz, W. F.; Reed, C. A.; Lee, Y. J.; Scheidt, W. R.; Lang, G. *J. Am. Chem. Soc.* **1982**, *104*, 6791–6793. (d) Barkigia, K. M.; Spaulding, L. D.; Fajer, J. *Inorg. Chem.* **1983**, *22*, 349–351. (e) Gans, P.; Buisson, G.; Duee, E.; Marchon, J.-C.; Erler, B. S.; Scholz, W. F.; Reed, C. A. *J. Am. Chem. Soc.* **1986**, *108*, 1223–1234. (f) Erler, B. S.; Scholz, W. R.; Lee, Y. J.; Scheidt, W. R.; Reed, C. A. *J. Am. Chem. Soc.* **1987**, *109*, 2644–2652. (g) Song, H.; Reed, C. A.; Scheidt, W. R. *J. Am. Chem. Soc.* **1989**, *111*, 6865–6866. (h) Song, H.; Reed, C. A.; Scheidt, W. R. *J. Am. Chem. Soc.* **1989**, *111*, 6867–6868. (i) Song, H.; Orosz, R. D.; Reed, C. A.; Scheidt, W. R. *Inorg. Chem.* **1990**, *29*, 4274–4282. (j) Scheidt, W. R.; Song, H.; Haller, K. J.; Safo, M. K.; Orosz, R. D.; Reed, C. A.; Debrunner, P. G.; Schulz, C. E. *Inorg. Chem.* **1992**, *31*, 939–941. (k) Scheidt, W. R.; Cheng, B.; Haller, K. J.; Mislankar, A.; Rae, A. D.; Reddy, K. V.; Song, H.; Orosz, R. D.; Reed, C. A.; Cukiernick, F.; Marchon, J.-C. *J. Am. Chem. Soc.* **1993**, *115*, 1181–1183.

(11) (a) Shimomura, E. T.; Phillippi, M. A.; Goff, H. M.; Scholz, W. F.; Reed, C. A. *J. Am. Chem. Soc.* **1981**, *103*, 6778–6780. (b) Itoh, K.; Nakahasi, K.; Toeda, H. *J. Phys. Chem.* **1988**, *92*, 1464–1468. (c) Gross, Z.; Barzilay, C. *Angew Chem., Int. Ed. Engl.* **1992**, *31*, 1615–1617. (d) Martin, P. C.; Arnold, J.; Bocian, D. F. *J. Phys. Chem.* **1993**, *97*, 1332–1338.

(12) (a) Lindsey, J. S.; Hsu, H. C.; Schreiman, I. C. *Tetrahetron Lett.* **1986**, *27*, 4969–4970. (b) Lindsey, J. S.; Schreiman, I. C.; Hsu, H. C.; Kearney, P. C.; Marguerettaz, A. M. *J. Org. Chem.* **1987**, *52*, 827–836.

(13) Li, X.-Y.; Czernuszewicz, R. S.; Kincaid, J. R.; Stein, P.; Spiro, T. G. *J. Phys. Chem.* **1990**, *94*, 47–61.

Table II. Infrared Frequencies and Their Normal Mode Assignments of CuTPP and Its Cation Radicals

CuTPP			CuTPP Cation Radical			
na	d_8	d_{20}	na	d_8	d_{20}	assignment
1598	1598	1564	1600	1599	1563	ϕ_4''
(1605)[a]	(1605)	(1578)				
1576	1576	1576	1560/1570	1548/1558		ν_{37} $\nu(C_\alpha–C_m)_{asym}$
(1586)	(1585)	(1588)				
1538	1504	1539	1516	~1497	1511	ν_{38} $\nu(C_\beta–C_\beta)$
(1552)	(1540)	(1543)				
1517	1504	1517	1485	1486	1486	ν_{39} $\nu(C_\alpha–C_m)_{sym}$
(1473)	(1447)	(1486)				
1490	1488	1378	1474		1384	ϕ_5''
(1513)	(1498)	(1388)				
1440	1441		1441	1441		ϕ^b
	1406		1429	1394	1432	ν_{40} ν(pyr quarter ring)
(1403)	(1370)	(1409)				
1345	1340	1331	1350	1340	1332	ν_{36} $\nu(C_m$–phenyl)
(1254)	(1244)	(1232)				
				1284		
1308	1263	1304	1289	1257	1286	ν_{41} ν(pyr half ring)$_{sym}$
(1331)	(1273)	(1331)				
			1232	1227		ϕ^b
1205	932	1207	1208	930	1191	ν_{52} $\delta(C_\beta H)_{sym}$
(1213)	(867)	(1189)				
1177	1178		1180/1190	1179/1189		ϕ_6''
(1199)	(1200)	(862)				
1157	1158		1165			ϕ
1071		1071	1072		1075	ν_{51} $\delta(C_\beta H)_{asym}$
(1093)	(783)	(1085)				
	1070			1070		ϕ_7''
(1057)	(1049)	(815)				
1004	1116	997	1004	1113	996	ν_{47} ν(pyr breathing)
(1023)	(1129)	(1031)				
1004	1003		1004	1002		ϕ_8
(941)	(940)	(912)				
995	992		996	990		$\phi_{8''}$
(939)	(944)	(912)				

[a] Values in parentheses are the calculated frequencies of NiTPP taken from ref 18. [b] Used to indicate either combination or overtone bands involving phenyl modes.

asymmetric C_α–C_m and the C_β–C_β stretching vibrations. The latter mode is found near 1600 cm^{-1} and is nearly insensitive to *meso-d_4* substitution. In the recent normal mode analysis of NiOEP,[13] the asymmetric C_α–C_m mode, ν_{37}, was calculated at 1637 cm^{-1} with a 17-cm^{-1} *meso-d_4* downshift. But no IR spectral feature is observed in this region. Rather a band of weak to medium intensity has been detected at about 1550 cm^{-1} for a number of M(OEP)s.[14] RR spectra of some 2,4-divinyl protoporphyrin(IX) derivatives[15] also show an extra IR-active band in this region, owing to the asymmetrical perturbation of the π electronic structure of the porphyrin macrocycle by the conjugating substituents. This perturbation lowers the effective symmetry of metalloporphyrin, thus activating some IR-allowed E_u modes in the RR spectrum. It is also known that the ~1550-cm^{-1} band is *meso-d_4* sensitive and shows an inverse correlation with the core sizes of metalloporphyrins.[14] These observations establish that the ~1500-cm^{-1} band has substantial C_α–C_m stretching character and should be assigned to the ν_{37} mode.[16]

The CuOEP$^{\bullet+}$ IR spectrum is more complex than that of the parent neutral porphyrin due to broadening and splitting of some of the bands, as indicated by the correlations drawn in the figure. The assignments are made with reference to CuOEP and the isotope shifts observed upon *meso* deuteration. The assignments are straightforward except for the complex envelope of bands at ~1460 cm^{-1}. We assign the 1466- and 1485-cm^{-1} components to the CH_2 scissor[13] and CH_3 asymmetric deformation modes,[17] shifted from their frequencies in CuOEP by mode crossing with the down-shifted ν_{39} skeletal mode. This assignment is based on the absence of *meso-d_4* shift for the fomer two bands and the appreciable downshift and splitting for the 1454-cm^{-1} band assigned to ν_{39}. The appearance of ν_{40} at 1429 cm^{-1}, identified by its 20-cm^{-1} *meso-d_4* shift, is also noted; this mode does not show up in the CuOEP spectrum.

The strong 1549-cm^{-1} band, which is the standard M(OEP)$^{\bullet+}$ marker band,[11a] is seen to be one component of ν_{37}. The other component, the 1573-cm^{-1} band, is likewise fairly strong, and the ν_{38} band is also seen to gain considerable intensity relative to that of the neutral parent compound. The splitting of ν_{37} and other E_u modes is attributable to solid-state effects, as revealed by the spectrum in $CDCl_3$ solution shown in Figure 2. A single band is now seen for ν_{37} as well as for ν_{38}, both showing the expected isotope shifts. Interestingly, the ν_{38} band is stronger than the ν_{37} band in solution. A marker band for M(OEP)$^{\bullet+}$ radicals has not previously been noted at about 1600 cm^{-1}, but reported IR spectra have all been taken on solids.[11]

B. CuTPP. Figure 3 shows IR spectra of CuTPP and its pyrrole-d_8 and phenyl-d_{20} isotopomers. Mode assignments are indicated in the figures and are tabulated in Table II. No metallo-TPP IR spectrum has previously been fully assigned, but the E_u modes of NiTPP were calculated in connection with the complete assignment of the RR spectra.[18] The calculated frequencies and isotope shifts are also given in Table II. Most of the assignments are in reasonable agreement with the NiTPP calculation, but there is one important exception. The strong band at 1345 cm^{-1} is assigned to ν_{36}, the C_m–phenyl stretch, although it is calculated

(14) Kincaid, J. R.; Urban, M. W.; Watanabe, T.; Nakamoto, K. *J. Phys. Chem.* **1983**, *97*, 3096–3101.

(15) (a) Choi, S.; Spiro, T. G.; Langry, K. C.; Smith, K. M. *J. Am. Chem. Soc.* **1982**, *104*, 4337. (b) Choi, S.; Spiro, T. G.; Langry, K. C.; Smith, K. M.; Budd, L. D.; La Mar, G. N. *J. Am. Chem. Soc.* **1982**, *104*, 4345.

(16) The likelihood of this assignment was acknowledged by Li et al.[13] who were, however, reluctant to introduce long-range interaction force constants, which would be necessary to separate ν_{37} from ν_{10} by the required ~100 cm^{-1}; these modes differ only in the phasing of the asymmetric C_α–C_m stretching coordinates.

(17) Hu, S.; Spiro, T. G. To be published.

(18) Li, X.-Y.; Czernuszewicz, R. S.; Kincaid, J. R.; Su, Y. O.; Spiro, T. G. *J. Phys. Chem.* **1990**, *94*, 31–47.

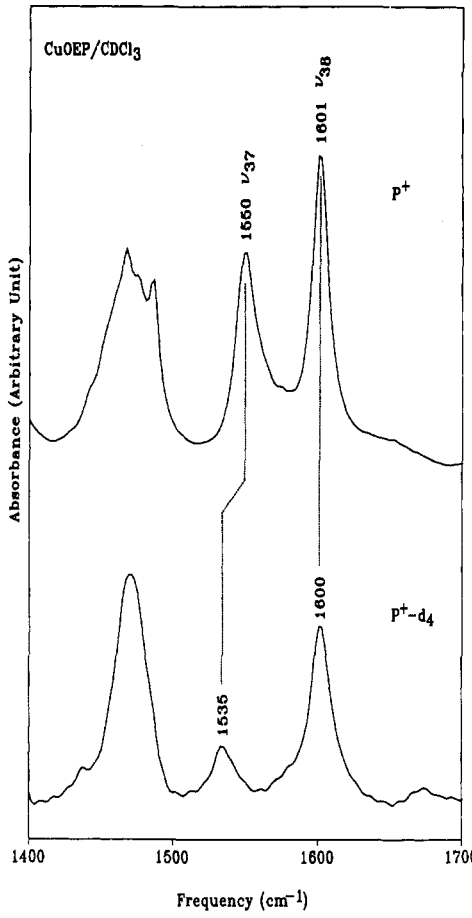

Figure 2. FT–IR spectra of the π-cation radicals for natural abundance (P^+) and *meso*-d_4 (P^+-d_4) CuOEP in chloroform-*d*. The solvent bands are numerically subtracted.

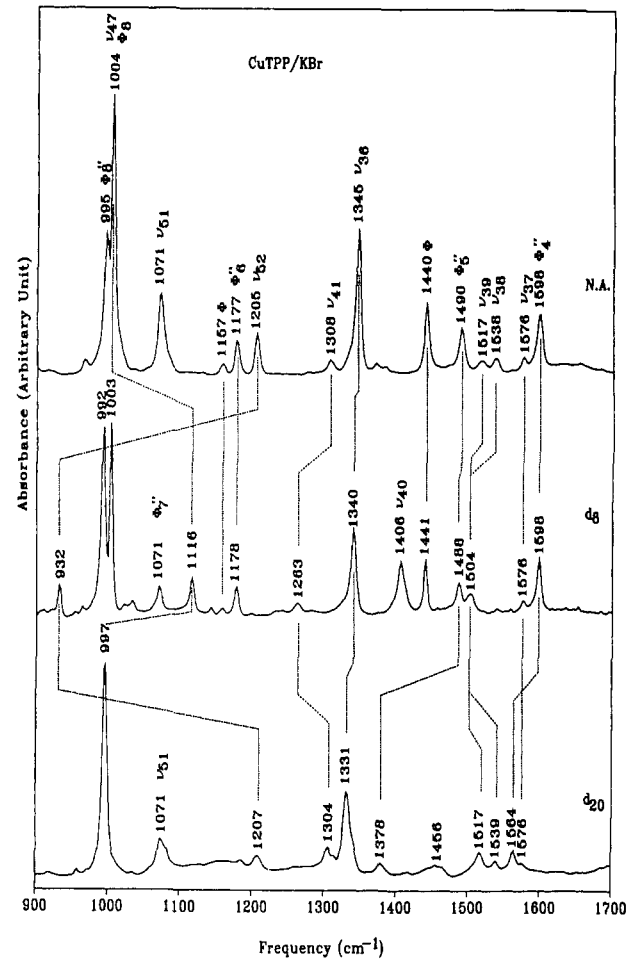

Figure 3. FT–IR spectra of natural abundance (na), pyrrole-d_8, and phenyl-d_{20} CuTPP isotopomers in KBr pellets.

at 1254 cm^{-1} in NiTPP, close to the A_{1g} and B_{2g} C_m–phenyl stretches, 1227 and 1267 cm^{-1}. The d_8 and d_{20} shifts of this band are similar to those calculated for ν_{36}, and an alternative assignment to the nearby pyrrole quarter-ring stretch, ν_{40} (calculated at 1331 cm^{-1}), is excluded because of the much larger expected d_8 shift. This mode is assigned to the 1308-cm^{-1} band, which shifts to 1263 cm^{-1} in the d_8 spectrum. The 90-cm^{-1} elevation of ν_{36} from its expected position implies interactions between the C_m–phenyl bond stretches on different methine bridges. Such interactions between bonds separated by four (for adjacent methine bridges) or six (for opposite methine bridges) intervening bonds were not included in the force field.[18]

Another point of interest is that more phenyl modes than expected appear in the IR spectrum, as judged from shifts and disappearances in the d_{20} spectrum. Only five phenyl modes are expected[18] above 900 cm^{-1}, ϕ_4''–ϕ_8'' (the double primes refer to the E_u phasing of the internal coordinates on the four phenyl ring; the other two phasings, B_{2g} and A_{1g}, belong to the Raman-active modes and are denoted with one prime and no prime, respectively). These are assigned to bands occurring at about the calculated frequencies of NiTPP,[18] but there are additional bands at 1004, 1157, and 1440 cm^{-1}. The first of these is revealed as underlying the ν_{47} skeletal mode when the latter is shifted out of the region by d_8 substitution. It is only 10 cm^{-1} above ϕ_8'' and may be due to one of the Raman modes, ϕ_8 or ϕ_8', rendered active by symmetry lowering in the solid state. The remaining two bands are too far from E_u correspondences to offer similar assignments; they may arise from overtone or combination modes involving the phenyl groups.

When the IR spectra of $CuTPP^{+\cdot}$ and its isotopomers were examined (Figure 4), very similar assignments could be made, as indicated in Table II. In contrast to CuOEP, ν_{37} and ν_{38} are weak in both the radical and the parent. The ν_{37} mode appears to split and to acquire some d_8 sensitivity in the radical. The spectra of CuTPP and $CuTPP^{+\cdot}$ in $CDCl_3$ solution are compared in Figure 5. In contrast to $CuOEP^{+\cdot}$, there are no changes for $CuTPP^{+\cdot}$ between solid and solution spectra, aside from some intensity variations and a 6-cm^{-1} upshift in ν_{41}. The ν_{37} and ν_{38} bands remain weak, and ν_{37} still appears to be split.

The most important result of these assignments is the recognition that the TPP π-cation radical marker band at 1289 cm^{-1} is the ν_{41} pyrrole half-ring stretch, which appears only weakly, at 1308 cm^{-1}, in the spectrum of the neutral parent.

Discussion

1. Marker Band Intensities and a_{1u} vs a_{2u} Radical Character. Having assigned the IR spectra, we are now in a position to understand the nature of the cation radical marker bands. For M(TPP)s the marker band at ~1280 cm^{-1} is the pyrrole half-ring stretch, ν_{41}. For M(OEP)s the marker band at ~1550 cm^{-1} seen (Figure 1) to be one component of the split ν_{37} bands associated with the asymmetric C_α–C_m coordinate. But the ν_{38} band at 1600 cm^{-1}, arising from C_β–C_β stretching, also gains appreciable intensity, and in solution (Figure 2), this band is stronger than the ν_{37} band.

These are markers of cation radical formation because they have much higher relative intensities than do the corresponding bands of the parent neutral porphyrins. This means that the dipole moment associated with the particular normal mde becomes much larger as a result of the removal of one electron from the HOMO. Figure 6 compares the eigenvectors of ν_{38}, calculated for NiOEP, and of ν_{41}, calculated for NiTPP, with the orbital pattern for the a_{1u} and a_{2u} orbitals. The a_{1u} orbital is antibonding with respect to the C_β–C_β bonds. It is therefore evident why the nuclear motion associate with ν_{38} should generate a large dipole

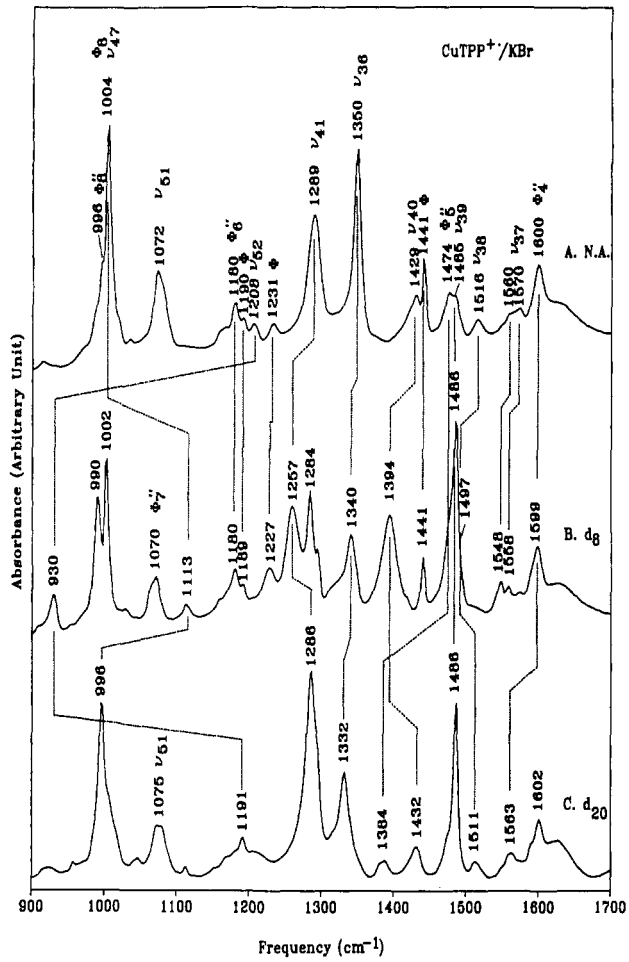

Figure 4. FT–IR spectra of the π-cation radicals for natural abundance (na), pyrrole-d_8, and phenyl-d_{20} CuTPP$^{\bullet+}$ isotopomers in KBr pellets.

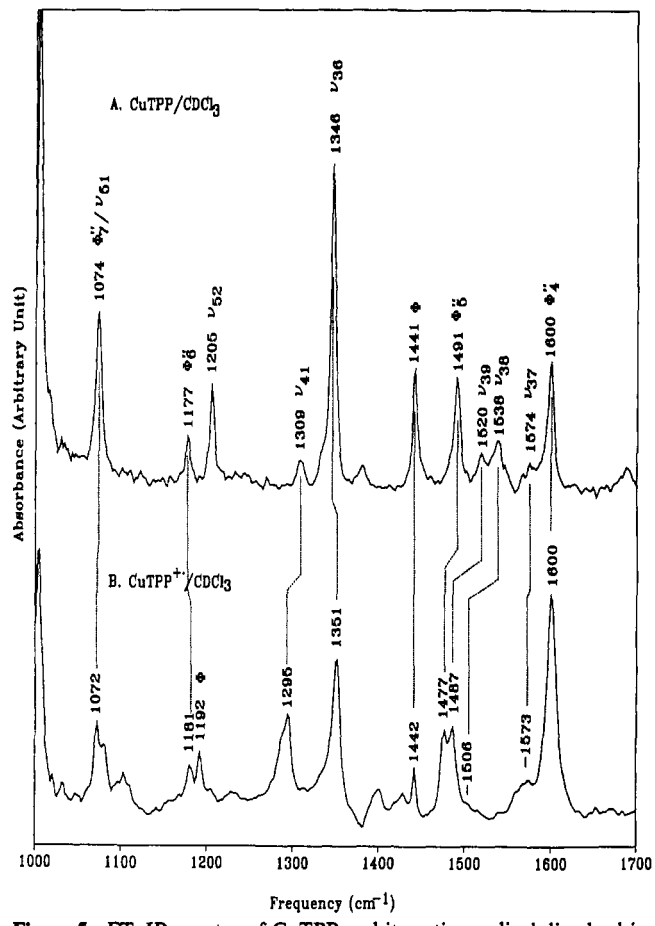

Figure 5. FT–IR spectra of CuTPP and its cation radical dissolved in chloroform-*d*. The solvent bands are numerically subtracted.

moment. As the C_β–C_β bonds on one side of the porphyrin contract and those on the other side expand, the electron shifts from the former to the latter to minimize the antibonding interaction. This effect is more pronounced for the π-cation radical than for the neutral porphyrin, since the latter is less polarizable inasmuch as the HOMO is filled.

The same argument applies to the interplay between the a_{2u} orbital structure and the ν_{41} mode of TPP. This mode involves the out-of-phase stretching of the C_α–N and C_α–C_β bonds. The a_{2u} orbital is antibonding for both sets of bonds. Consequently, the E_u phasing of the pyrrole half-ring stretch would shift the electron from one side of the porphyrin to the other. This polarization effect is diagramed schematically in Figure 7 for both the a_{1u} and a_{2u} orbitals. Thus, the different marker band enhancements for OEP and TPP π-cation radicals can be understood in terms of the match between the HOMO antibonding pattern and the shape of the eigenvectors.

The enhancement mechanism of ν_{37}, which gives the strongest intensity for CuOEP$^{\bullet+}$ in the solid state is less transparent. This mode principally involves the asymmetric C_α–C_m stretch, a coordinate that does not directly affect bonding or antibonding character in the a_{1u} HOMO, which has a node at C_m. Part of its intensity is attributable to vibrational mixing with the nearby ν_{38}, which introduces some C_β–C_β character. But a more interesting explanation is mixing of a_{2u} character into a_{1u} cation radicals, an effect shown by MNDO/3 calculation to produce a substantial orbital coefficient on the C_m atoms (Figure 8);[19] adjacent C_α–C_m bonds have bonding and antibonding interactions in the HOMO. A bond-alternate distortion is predicted, with bond length inequivalences of ~0.04 Å between adjacent C_α–C_m or C_α–N bonds,[19] in excellent agreement with the crytal structure

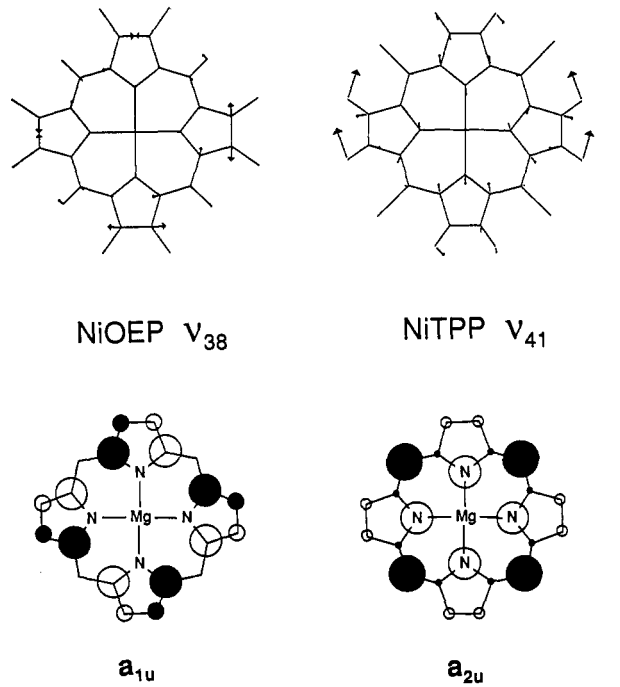

Figure 6. Comparison of the metalloporphyrin a_{1u} and a_{2u} orbitals with the ν_{38} eigenvector of NiOEP and the ν_{41} eigenvector of NiTPP showing the matching of the antibonding node patterns and vibrational phases. The orbital diagrams are adapted from ref 9c, and the eigenvectors are calculated using the force fields of NiOEP[13] and NiTPP.[18]

of ZnOEP$^{\bullet+}$.[10j] The asymmetric C_α–C_m stretch maps onto this bonding/antibonding pattern, and E_u phasing is expected to produce a large dipole moment, also diagramed in Figure 8. This mechanism appears to apply with greater force to the solid phase,

(19) Prendergast, K.; Spiro, T. G. *J. Phys. Chem.* **1991**, *95*, 9728–9736.

Table III. Comparison of Resonance Raman and Infrared Frequencies of CuOEP and CuTPP and Their π-Cation Radicals

	CuOEP (ΔCuOEP$^{+\cdot}$)		CuTPP (ΔCuTPP$^{+\cdot}$)	
	RR[a]	IR	RR[a]	IR
$\nu(C_\alpha–C_m)_{asym}$	ν_{10} 1637 (5[b])	ν_{37} 1551 (1)	ν_{10} 1582 (–4)	ν_{37} 1574 (1)
$\nu(C_\beta–C_\beta)$	ν_2 1592 (–21)	ν_{38} 1601 (–1)	ν_2 1562 (32)	ν_{38} 1538 (32)
$\nu(C_\alpha–C_m)_{sym}$	ν_3 1503 (4)	ν_{39} 1476 (22)	ν_3	ν_{39} 1520 (14)
ν(pyr quarter ring)	ν_{29} 1406	ν_{40}	ν_{29}	ν_{40} 1406 (12)[c]
ν(pyr half ring)	ν_4 1378 (15)	ν_{41} 1368 (18)	ν_4 1365 (10)	ν_{41} 1309 (14)

[a] RR frequencies are taken from ref 9c. [b] The numerical values indicate the downshift and upshift (– sign) from the neutral species to the π-cation radical. [c] The mode is observed for CuTPP–d_8.

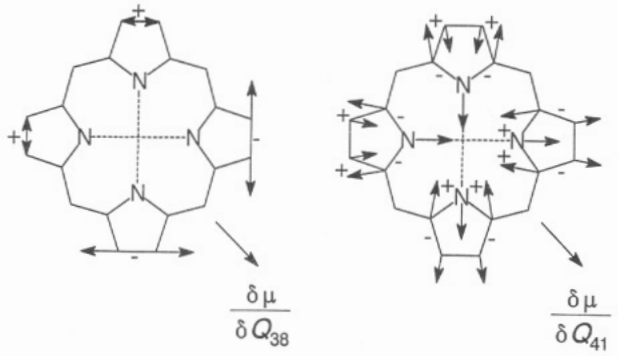

Figure 7. Diagram of the molecular dipole moment derivative for metalloporphyrin π-cation radicals. The vibrationally induced charge redistribution on the a_{1u} and a_{2u} orbitals are shown with respect to the $C_\beta–C_\beta$ stretching vibration (ν_{38}) and the pyrrole half-ring stretching vibration (ν_{41}).

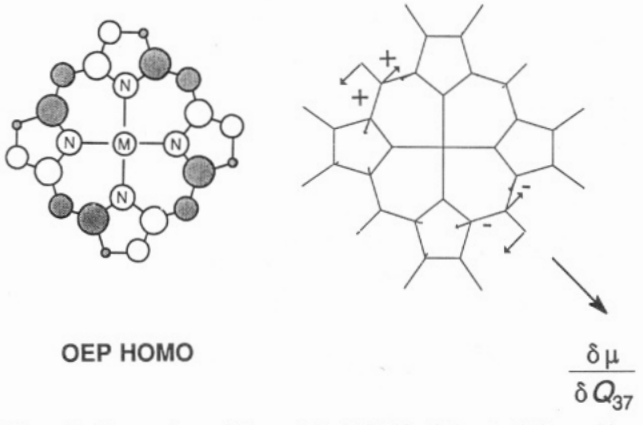

Figure 8. Comparison of the a_{1u}-like HOMO of the zinc(II) porphine cation radical with the ν_{37} eigenvector of NiOEP, on which the molecular dipole moment is superimposed. The a_{1u}-like orbital is adapted from ref 19, while the eigenvector is calculated using the force field of NiOEP.[13]

where ν_{37} is stronger than ν_{38}, than to the solution phase, where ν_{38} is stronger. This difference is consistent with the idea[9c] that the bond-alternant distortion is a dynamical one in solution, as evidenced by anomalously polarized A_{2g} modes with depressed freqencies,[9c] signaling a pseudo-Jahn–Teller effect, but that the distortion becomes trapped upon crystallization.

2. E_u Mode Frequency Shifting and Splitting in Cation Radicals. Figure 1 shows the splitting of many E_u modes of CuOEP$^{+\cdot}$ in the solid state, but the splitting is removed, at least in the case of the ν_{37} band, in solution (Figure 2). This observation implies a lowering of the effective symmetry of the porphyrin upon crystallization. The bond-alternant distortion, mentioned in the previous section, is not in itself sufficient to split the E_u modes since C_4 symmetry is maintained. But, the crystal structures of ZnOEP$^{+\cdot}$ and NiOEP$^{+\cdot}$ cation radicals show cofacial stacking of pairs of porphyrin rings, with D_2 symmety for the dimers.[10j] Thus, the splitting of the E_u modes is attributed to dimer formation upon crystallization. No extra splittings are seen for CuTPP$^{+\cdot}$ in the solid state (the apparent splitting of the weak ν_{37} band is maintained in solution), consistent with the absence of tightly cofacial dimers in TPP$^{+\cdot}$ cation radical crystals; the mean interplanar distance is 5.43 Å in the CuTPP$^{+\cdot}$ crystal compared with 3.19 Å in the NiOEP$^{+\cdot}$ crystal. The weaker dimerization may account for the saddle structure of crystalline CuTPP$^{+\cdot}$, although it is a structure in solution.[10c] It is possible that the 6-cm^{-1} solid-state downshift of ν_{41} is a reflection of the saddle geometry, which might alter the pyrrole half-ring stretch kinematically. More direct effects of out-of-plane distortion are expected in the low-frequency region of the vibrational spectra; this region has not yet been examined for porphyrin radicals.

Table III compares RR and IR frequencies for skeletal modes of the CuOEP and CuTPP neutral and cation radicals. There is a reasonable correspondence between the frequency shifts for modes associated with a given local coordinate. In particular, the pyrrole half-ring stretches, ν_4 and ν_{41}, both shift down by 10–20 cm^{-1} upon radical formation in both CuOEP and CuTPP, while the asymmetric $C_\alpha–C_m$ modes, ν_{10} and ν_{37}, have frequencies that are nearly insensitive to radical formation. Interesting differences are found among the $C_\beta–C_\beta$ (ν_2 and ν_{38}) and the symmetric $C_\alpha–C_m$ (ν_3 and ν_{39}) stretches, however. For CuTPP, both ν_2 and ν_{38} shift down in frequency, reflecting the $C_\beta–C_\beta$ bonding character of the a_{2u} orbital; ν_{39} also shifts down (ν_3 has not been identified in the RR spectrum), reflecting the $C_\alpha–C_m$ bonding character. In the case of CuOEP, however, the Raman bands show the expected electronic effects but the IR bands do not. ν_2 shifts *up*, on radical formation, reflecting the $C_\beta–C_\beta$ antibonding character of the a_{1u} orbital, while ν_3 shifts down only slightly, since there is a node at C_m and mixing-in of a_{2u} character produces an asymmetric $C_\alpha–C_m$ nodal pattern (see Figure 8). But in the IR spectrum, the putative $C_\alpha–C_m$ symmetric stretch, ν_{39}, shifts down in frequency, while the $C_\beta–C_\beta$ stretch, ν_{38}, is unshifted. We attribute these anomalies to coordinate mixing among the E_u modes ν_{37}, ν_{38}, and ν_{39}, all of which are fairly close in frequency. Mixing among the Raman modes is restricted by the greater frequency spread and, in the case of ν_{10} (a B_{1g} mode), by symmetry. The bonding changes, which give a clear signature in the Raman frequencies, may be obscured in the IR frequency pattern by changes in coordinate mixing.

Acknowledgment. This work was supported by Grant GM33576 from the National Institutes of Health. We would like to thank Mr. Arka Mukherjee for his assistance in plotting the eigenvectors of NiOEP and NiTPP, shown in Figures 6 and 8.